Temperature driven semiconductor–metal transition and structural changes in liquid As_2Se_3

TOPICAL REVIEW

Temperature driven semiconductor–metal transition and structural changes in liquid As_2Se_3

Shinya Hosokawa[1,2,4] **and Kozaburo Tamura**[3]

[1] Department of Engineering, Hiroshima Institute of Technology, Hiroshima 731-5193, Japan
[2] Institut für Physikalische-, Kern-, und Makromolekulare Chemie, Philipps Universität Marburg, D-35032 Marburg, Germany
[3] Department of Materials Science and Engineering, Graduate School of Engineering, Kyoto University, Kyoto 606-8501, Japan

E-mail: hosokawa@cc.it-hiroshima.ac.jp

Abstract
Intensive experimental investigations have been performed on a typical liquid semiconductor As_2Se_3 over a wide temperature range under pressure, such as electrical conductivity, optical absorption coefficient, density, x-ray absorption fine structure, and x-ray diffraction measurements. With increasing temperature, it was found that liquid As_2Se_3 undergoes a semiconductor–metal transition at about 1000 °C, which is clearly seen in the electrical conductivity and optical absorption measurements. This transition is accompanied by significant structural and thermodynamical changes. The volume of the system apparently contracts near the transition temperature. The structural changes are observed especially in the intermediate-range order or the prepeak in the total structure factor characteristic to this glass-forming liquid. X-ray absorption fine structure (XAFS) and x-ray scattering results strongly suggest a formation of new As–As bonds in addition to the original As–Se bonds in the high-temperature metallic region. These experimental results are carefully discussed by comparing to theoretical results from an *ab initio* molecular dynamics (MD) simulation. Some new insights can be realized from this computational work. For example, a small portion of homopolar bonds already exist in the semiconducting region, and twofold coordinated As atoms existing in a chain structure with twofold coordinated Se atoms play a very important role for the metallization of this liquid. Some limitations of the MD simulation are also pointed out.

[4] Author to whom any correspondence should be addressed.

Contents

1. Introduction

The high temperature crystal phase of arsenic triselenide (As_2Se_3) consists of layers [1]. In each layer, As–Se spiral chains parallel to the c-axis are bridged by Se atoms (see figure 1). Each As atom is surrounded by three Se atoms, and each Se atom by two As atoms. Only the As–Se heteropolar bonds form the network structure.

Glassy As_2Se_3 is well known as a prototype semiconductor having a strong glass-forming tendency; it is recognized that this concentration is the so-called stiffness threshold composition where the average coordination number $\langle r \rangle$ is 2.4 [2, 3], i.e., the average number of constraints is equal to the degree of freedom. Physical properties of glassy As_2Se_3 have been intensively investigated from both the experimental and theoretical points of view [4]. For glassy As_2Se_3, x-ray [5], electron [6] and neutron [7] diffraction measurements showed that the interatomic distance r_1 is almost the same as that of 0.242 nm in the crystalline phase [8], and the averaged coordination number N_1 is around 2.5. Hence it is widely believed that a short-range order (SRO) in glassy As_2Se_3 is a chemically ordered covalent network similar to the crystal, i.e., threefold coordinated As and twofold coordinated Se atoms are covalently bound to each other. The results of x-ray absorption fine structure (XAFS) [9], Raman spectroscopy [10] indicated no contradiction against this model. Such a crystal-like SRO is also conserved in liquid As_2Se_3 near the melting point, which is supported by neutron diffraction [11], XAFS [9] and infrared absorption [12] measurements. The occurrence of a prepeak (or a first sharp diffraction peak) around 12 nm^{-1} in the total structure factor, $S(Q)$, in both glassy and liquid As_2Se_3 is considered as clear evidence of intermediate-range order (IRO), which has attracted much interest. However, the origin of the prepeak or the IRO is still open to discussion.

Due to the preservation of the covalent bonding, the main feature of the electronic structure of liquid As_2Se_3 near the melting temperature is semiconducting, which was confirmed with the results of electrical conductivity, thermoelectric power, and optical absorption measurements [13].

As the temperature increases, the breaking of the covalent bonds occurs, as confirmed by the results of viscosity measurements [14, 15]. This disruption changes the electronic structure of liquid As_2Se_3, including the generation of defect states with increasing temperature. In fact, Edmond [13] carried out electrical conductivity, σ, measurements up to 750 °C and found that
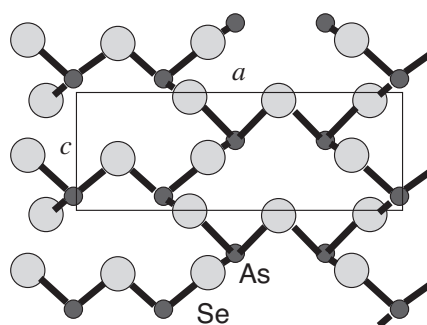
Figure 1. Schematic view (one layer) of high-temperature phase crystalline As_2Se_3.

σ significantly increases by raising temperature, and beyond about 600 °C there appears a deviation to higher σ from an Arrhenius behaviour typical for semiconductors. Moreover, his measurement of optical absorption coefficient, α, revealed that the energy gap, defined as an energy where $\alpha = 100$ cm^{-1}, rapidly decreases with temperature from 1.30 eV (288 °C) to 0.50 eV (597 °C). At normal pressure, however, the high vapour pressure of As_2Se_3 prevents one from making further investigations of this system at higher temperatures.

In this decade, the present authors and co-workers carried out several experiments for liquid As_2Se_3 at high temperatures under pressure. The electrical conductivity [16] and the optical absorption [17] measurements were made to investigate the electronic states, the density [18] for the thermodynamic property, and the x-ray diffraction [18, 19] and the XAFS [20] for the structural information. From these experiments we have visualized a semiconductor-to-metal (SC–M) transition around 1000 °C accompanied by an apparent volume contraction and a large structural change. Shimojo *et al* [21, 22] have performed an *ab initio* molecular dynamics (MD) simulation to theoretically investigate this SC–M transition in liquid As_2Se_3 at high temperatures.

In this paper we shall review our experimental studies and discuss them together with the theoretical results. We have organized this article as follows: in the next section, experimental procedures will be given in the subsections for each experiment performed under high pressure and temperature. In section 3, experimental results will be shown in each subsection for each property. In section 4, we will discuss the present experimental results by comparing the *ab initio* MD simulation, and give the summary in the last section.

2. Experimental purposes and procedures

In order to suppress the evaporation of the liquid As_2Se_3 sample at high temperatures, we carried out the experiments at high pressures of several tens of bars. The underlying experimental principle of these studies was based on the well known concept of an internally heated high-pressure vessel which has proven successful in many measurements of equation of state data and electronic properties under *static* conditions of high temperature and high pressure [23].

The general technique is as follows. High-purity grade noble gas (Ar or He) was used as the pressurizing medium, and the pressure was measured with Heise gauges. He gas was used for the x-ray experiments due to the low absorption constant for hard x-rays in the energy range of our experiments. High temperatures were generated using resistant heaters made of Mo or W wire. The small size of the heating systems allowed us to locally heat up the sample to high temperatures up to 1700 °C in a small volume inside the high-pressure vessels.
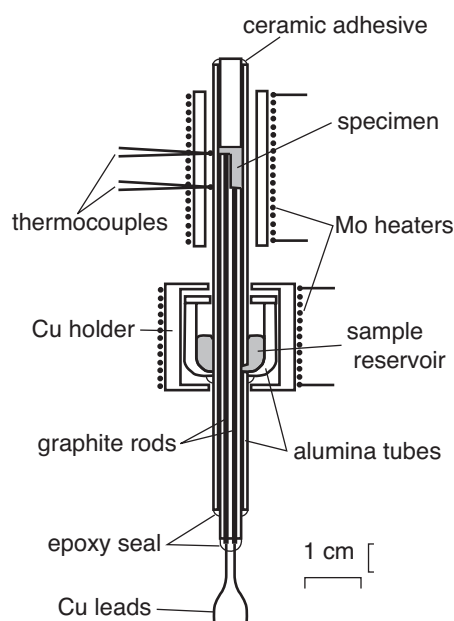
Figure 2. The sample cell used for the measurements of electrical conductivity. The vertical scale is reduced to half of the horizontal one.

The temperature of the sample was measured with two or three thermocouples. Bridgeman-type high-pressure leadthroughs were provided for the heaters and thermocouples through the flange of the vessel. Water cooling jackets were placed outside the vessel to keep the vessel temperature near room temperature. Details are given elsewhere [23, 24].
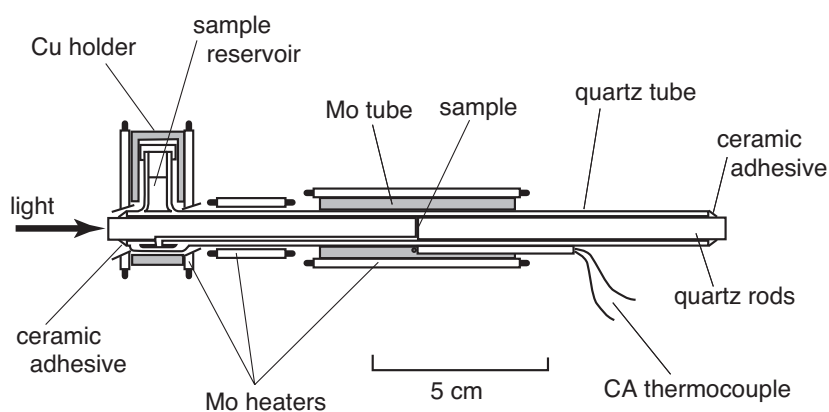
The extension of this basic concept to our several studies was, however, an extremely difficult task. In the following subsections, we would like to explain our respective technique for each experiment.

2.1. Electrical conductivity

An electrical conductivity measurement is, needless to say, essential to examine the electronic transport properties. The measurements in liquid As_2Se_3 were performed in a temperature range of 600–1400 °C under high pressure up to 600 bar [16]. The high-pressure vessel used for the experiments is shown in figure 1 of [25].

Figure 2 shows the sample cell placed in the vessel. Due to the strongly corrosive nature of the liquid As_2Se_3 sample at high temperatures, high-purity (99.9%) alumina tubes have to be used for the cell material and high-purity (99.9999%) graphite rods for the electrodes. A four-bore alumina tube with an outer diameter of 4 mm and a bore diameter of 0.8 mm was inserted in an outer alumina tube. Another closed-end alumina tube was located outside the cell, and serves as a sample reservoir. All of the alumina parts were cemented with a high-temperature ceramic adhesive (SEM-COM Co. Inc. type SCE-1), and the electrodes were sealed with epoxy adhesive where low temperature was kept during the experiment. The total length of the cell was about 160 mm. The measurements of electrical conductivity were performed by the normal four-probe method using the four graphite rods.

We used a commercial sample with a purity of 99.999%. High temperatures were achieved using an Mo resistance wire with a diameter of 0.7 mm, which was wound outside an alumina

Cu holder   sample
reservoir

Mo tube   sample   quartz tube

ceramic
adhesive

light

ceramic
adhesive

Mo heaters   5 cm   CA thermocouple

quartz rods

Figure 3. The optical cell of our own design made of quartz with a sample thickness of about 300 nm.

tube. The temperature was measured with two Pt–30%Rh:Pt–6%Rh thermocouples, which were in touch with the outer wall of the cell. The sample reservoir was heated up to slightly above the melting temperature using another Mo heating element.

The following procedure is how to completely fill the sample space with the liquid As_2Se_3 sample. First, the solid sample was put into the sample reservoir. After closing the high-pressure seals, the entire assembly was evacuated, and the sample space was heated up to 400 °C. Then, the solid sample loaded in the sample reservoir was fused by heating it to 320 °C. At this stage no gas except rarefied vapour of the sample remained inside the alumina cell and the reservoir was filled with the liquid sample. Finally, the high-pressure vessel was pressurized with Ar gas of two or three bar that was sufficient to reinforce the liquid sample through a small channel between the outer and inner alumina tubes and to fill the sample space as shown in figure 1. Ar gas could not go into the sample space due to no leakage in the cell. Once the cell had been filled, the temperature of the reservoir was maintained near the melting temperature of 250 °C. Since the pressure balance between the liquid sample and the compressed Ar gas outside was achieved through the sample reservoir, no mechanical force was applied to the cell. The sample reservoir was encased with a Cu holder in order that the As_2Se_3 vapour could not escape. This procedure is, in principle, universal among the several experimental techniques reviewed in this paper.

2.2. Optical absorption coefficient

It is obvious that useful information on the electronic structure can be obtained from studies of optical properties, particularly from measurements of optical absorption coefficient, α, performed in the wide absorption range. Absorption spectra in the low absorption range give information about defects produced by the bond scission, and those in the high absorption range about the valence–conduction interband transition.

The measurements of α beyond 10^5 cm^{-1} definitely require a sample thickness of some 100 nm. It should be noted that it is extremely difficult to construct an optical cell keeping such a thin liquid film with high vapour pressure stable. We measured α of liquid As_2Se_3 in a wide absorption range from 8 to 3×10^5 cm^{-1} [17] up to 900 °C at 20 bar.

Figure 3 illustrates the optical cell of our own design with a sample thickness of 200 nm. Two quartz rods with a diameter of 6.5 mm and a length of 80 mm were put into a quartz tube with an inner diameter of 6.5 mm, an outer diameter of 8 mm, and a length of 150 mm.
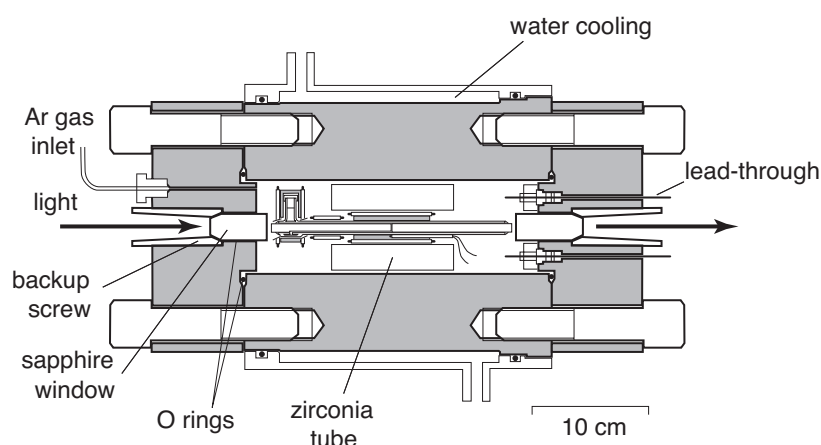
Figure 4. The high-pressure vessel with two optical sapphire windows used for the measurement of optical absorption coefficient.

The ends of the rods were polished to have optically flat surfaces. The cell had a uniform gap between the rods as a sample space, where the liquid sample was introduced from the sample reservoir. We prepared six cells with the optical path-lengths of about 0.5 mm, 40, 4, 1 μm, and 300 nm, to cover a wide α range. The quartz rods and the tube were cemented with high-temperature ceramic adhesive (Vitta type P-1015). A detailed description of how to construct this cell is given elsewhere [26].

The sample was heated with an Mo resistance wire. In order to reduce the temperature gradient around the sample, an Mo tube was placed between the cell and the heater. The temperature was measured with two chromel–alumel (CA) thermocouples attached on the outside wall of the cell through the holes drilled in the Mo tube.

The measurements were carried out at a high pressure of 20 bar. For this, we used a high-pressure vessel with two optical windows made of sapphire, which is illustrated in figure 4. The incident and transmitted photons passed through the sapphire windows with a thickness of 55 mm and a diameter of 20 mm placed in both flanges. Each window was supported with a conical area of a backup screw. A Bridgeman-type high-pressure seal was applied to the outside of the window. The space between the heaters and the inner wall of the high-pressure vessel was filled with thermally insulating materials, such as zirconia and alumina tubes.

We measured α using a Jasco CT-25GD spectrometer in a wide photon-wavelength range from 330 to 2500 nm, which corresponds to the photon energy ($\hbar\omega$) range from 0.50 to 3.75 eV. In order to obtain α from the measured optical transmittance spectra, we took account of various effects in correction, of which the following four were very important: optical reflectance, interference fringes, temperature variations for the sample thickness, and those of the optical absorption of the quartz cell.

Recently, Sakaguchi and Tamura made a further improvement for the optical cell [27], which required almost no corrections of the temperature changes in the sample thickness and in the optical absorption of quartz.

2.3. Density

Density is the most fundamental thermodynamic quantity of materials. The sets of its temperature and pressure dependence enable us to widely evaluate thermodynamic functions.
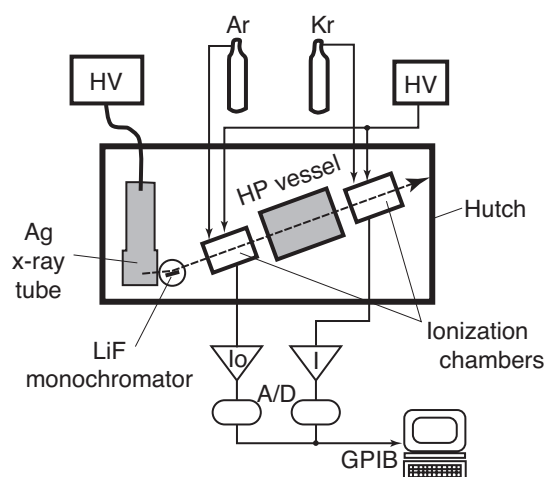
Figure 5. Schematic view of the apparatus for the density measurement under high temperature and high pressure using the x-ray absorption method. HV: high-voltage power supply.

It is sensitively affected by a cohesive energy of constituent atoms or electronic states of materials. It is well known that some chalcogenide liquids show anomalous density changes (volume contraction with increasing temperature) on the SC–M transition [28]. Moreover, the density data are essential for analysing, e.g., diffraction data to evaluate pair distribution function.

Due to the strong corrosive nature of liquid As_2Se_3 and the extreme condition of high pressure, normal methods for the density measurements which have been used so far, i.e., the volume method, the Archimedean method and the γ-ray absorption method, can only be employed with difficulty. The density measurements on liquid As_2Se_3 were carried out by the x-ray absorption method, which we developed for expanded fluid Se at high temperatures and high pressures [29].

Figure 5 shows a schematic view of the apparatus. X-rays (Ag Kα, 22.16 keV) emitted from a commercial x-ray tube with an Ag target (Philips model PW 2249/20) and monochromatized with an LiF crystal were used as an incident beam. The x-ray tube was operated at 45 kV and 25 mA. The sample was located in a high-pressure vessel. The intensity of the incident beam, I_0, and that of the transmitted beam, I, were measured using two ionization chambers with the path-lengths of 17 cm filled with pure Ar and Kr gases, respectively. Each current signal detected by the chambers was amplified, digitized, and then averaged over 100 times.

The experimental conditions of high temperatures up to 1600 °C and high pressures up to 700 bar were achieved with an internally heated high-pressure vessel, whose outline is given in figure 1 of [20] or figure 3 of [29]. The construction of this high-pressure vessel is similar to that for the optical absorption measurement given in figure 3. The incident and transmitted x-ray beams passed through Be windows of 10 mm in thickness and 8 mm in diameter. Each window had a tapered shape, and was supported with a tapered area of a backup screw.

The liquid As_2Se_3 sample must be contained in a cell made of a material that is highly transparent to hard x-rays and resistant to chemical corrosion with the hot sample. For this purpose, we developed a cell made of polycrystalline sapphire (NGK type G-30, 31). The cell assembly is illustrated in figure 6. Two sapphire tubes with an outer diameter of 4.5 mm and an inner diameter of 3 mm were prepared. The lengths of the long and short tubes were
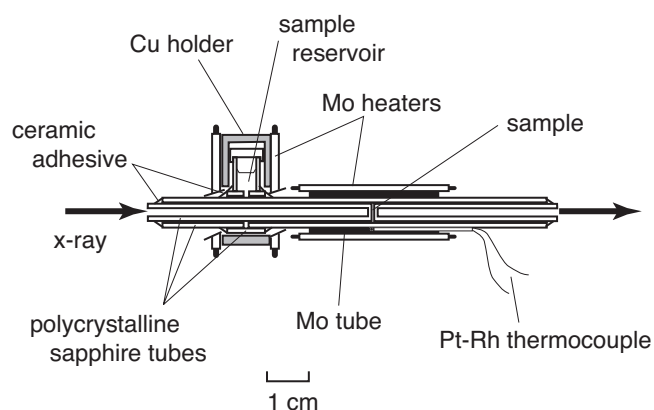
Figure 6. The cell assembly made of polycrystalline sapphire used for the density and XAFS measurements.

55 and 45 mm, respectively. Each tube had a closed end, which was polished to a thickness of 0.25 mm in order to improve the efficiency of x-ray transmission. These tubes were inserted into another tube with an inner diameter of 4.5 mm, an outer diameter of 6 mm, and a length of 90 mm, in such a way that the closed ends of the inner tubes faced each other with a narrow and uniform gap of 0.2 mm between them. The heating system was similar to that used for the optical absorption measurement given in the previous subsection. We used three Pt–30%Rh:Pt–6%Rh thermocouples to monitor the temperature of the sample.

The absorption data I/I_0 are expressed as

$$I/I_0 = C \exp[-(\mu t)_{Be} - (\mu t)_{He} - (\mu t)_{cell} - (\mu t)_{sample}],$$

where C is an instrumental constant, and μt the x-ray absorbance. The subscripts on the absorbance indicate that each μt is respectively that of the Be windows, the compressed He gas, the sapphire cell, and the liquid As_2Se_3 sample. In order to remove the effect of the absorption except for the sample, their total absorbance without the sample was separately measured with varying temperature and pressure. The density of liquid As_2Se_3, ρ, is derived from $(\mu t)_{sample}$ as
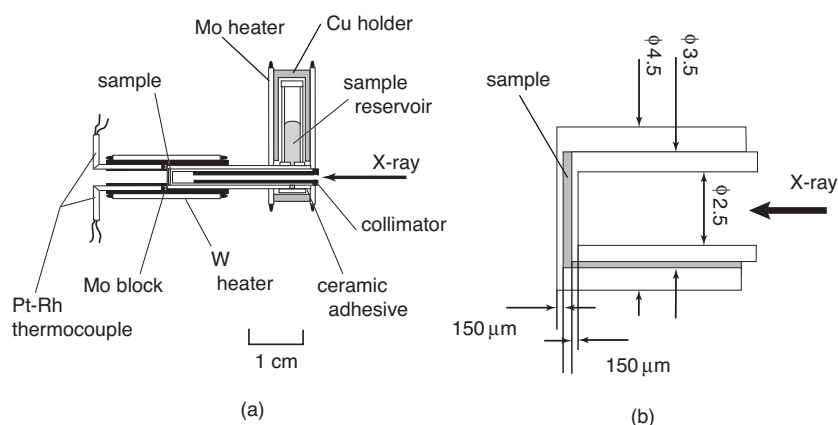
$$(\mu t)_{sample} = (\mu/\rho)_{sample} \rho t,$$

where $(\mu/\rho)_{sample}$ is the mass absorption coefficient of As_2Se_3, and t the sample thickness.

2.4. X-ray absorption fine structure (XAFS)

It is obvious that XAFS measurements give useful structural information on the local environment around each of the constituent atoms in alloy systems. There has, however, been little application of the XAFS technique to liquids at high temperatures so far, because it is difficult to keep a thin liquid sample stable in a cell. Crozier et al [9] performed XAFS measurements on liquid As_2Se_3 using a sample cell made of boron nitride. The measurements were, however, limited at temperatures near the melting point due to the high vapour pressure.

Using the same high-pressure vessel and the polycrystalline sapphire cell as in the density measurements described in the previous subsection, we carried out the XAFS measurements in a wide temperature range up to 1400 °C under pressure up to 60 bar [20]. The measurements were performed using an XAFS spectrometer installed at the beamline BL-10B of the Photon Factory in Tsukuba, Japan, in a usual transmission mode. With an Si(311) channel-cut

Figure 7. (a) The construction of the single-crystal sapphire cell (Tamura-type cell) used for the x-ray diffraction studies of liquid As_2Se_3. (b) Details of the sample space are shown on an enlarged scale.

monochromator, an energy resolution of 1.1 eV at 9 keV was achieved with a typical photon flux of 10^9 photons s^{-1} when the storage ring was operated at 2.5 GeV and 300 mA. The reproducibility of the energy axis was 0.3 eV around the As and Se K edges. The intensity of the incident beam, I_0, and that of the transmitted beam, I, were monitored using two ionization chambers with a path-length of 17 cm filled with 85%N_2–15%Ar mixture and pure Ar gases, respectively. The integration time for the photon counting was 2 s per point. In a typical run, it took 40 min to survey the region around each K edge.

In order to obtain the XAFS function $\chi(k)$ as a function of photoelectron wavevector k, the background level for higher shells and the absorption for an isolated atom were subtracted from the observed absorption, $-\ln(I/I_0)$, using a Victreen fit and a cubic spline technique. Details of the data analysis were given in the previous paper [30].

2.5. X-ray diffraction

X-ray scattering study has been used for investigating the structure of non-crystalline materials for a long time; structural information on both local and intermediate ranges can be obtained. The latter is lacking in the XAFS investigations due to the limited lifetime of the photo-excited electrons during the XAFS process. Since a θ–θ diffraction geometry using a free surface of liquid has only been available for measuring the liquid states [31] so far, however, this technique has a strong limitation that the vapour pressure of the sample should be very low. Thus, this is not suited to liquid As_2Se_3. This limitation has skilfully been solved by using the so-called Tamura-type cell, which has been described elsewhere [24].

Liquid As_2Se_3 must be contained in a cell made of a single-crystal sapphire, which is transparent to x-rays and resistant to chemical corrosion by hot liquid As_2Se_3. Details of the cell are illustrated in figure 7(a), and the construction around the sample is shown in figure 7(b) on an enlarged scale. A closed-end sapphire tube with an inner diameter of 2.5 mm, an outer diameter of 3.5 mm, and a length of 27 mm was put into another closed-end tube with an inner diameter of 3.5 mm, an outer diameter of 4.5 mm, and a length of 26 mm. The sapphire components were connected with a high-temperature ceramic adhesive (SEM-COM Company Inc., Type SCE-1) providing a uniform gap between the closed ends of the tubes as shown in figure 7(b). The thickness of the closed end of each tube through which x-rays passed was 150 μm, and the gap was about 200 μm.
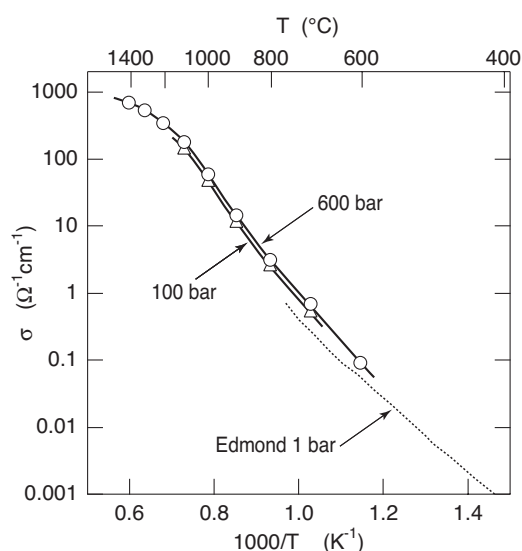
Figure 8. Logarithmic plots of electrical conductivity σ at pressures of 100 and 600 bar as a function of reciprocal temperature $1/T$. Also given as a dashed curve is a previous result at normal pressure measured by Edmond [13].

In measuring x-ray diffraction from the liquid sample contained in the sample cell, the problem was how to discriminate the diffraction of the sample from that of the sapphire cell. This was solved by employing the following procedure on assembling the cell. In the first step, both the sapphire tubes were manufactured so that their c axes were parallel to the direction of the primary x-ray beam. When incident x-rays were diffracted by the closed ends, Laue spots with a triple symmetry were observed in the plane perpendicular to the c axis. Each closed-end tube rotated independently around the c axis until no Laue spots appeared in the horizontal direction. After these conditions were fulfilled, the tubes were cemented. Since the detector moved on the horizontal plane, the diffracted x-rays had no Bragg or coherent components originating from the sapphire cell.

The cell was heated by a heating element made of an Mo wire with a diameter of 0.4 mm. As seen in figure 7(a), the Mo heater was set around an Mo block. Since a slit was cut on the left-hand side of the Mo block, diffracted x-rays were able to go out through it. The temperature of the sample was monitored with two Pt–30%Rh:Pt–6%Rh thermocouples, which were located in the holes of the Mo block and were in close contact with the wall of the closed end of the outer sapphire tube. A collimator made of Mo with an inner diameter of about 1 mm and a length of 23 mm was put into the inner closed-end tube. The cell and the heaters were supported by alumina discs.

The cell and heaters were placed in a high-pressure vessel with fixed Be windows (figures 2 and 3 of [26]) or continuous Be windows (figures 1 and 2 of [32]).

3. Experimental results

3.1. Electronic property

Figure 8 shows the logarithmic plots of electrical conductivity σ at pressures of 100 and 600 bar as a function of reciprocal temperature $1/T$. Also given as a dashed line is a previous result at
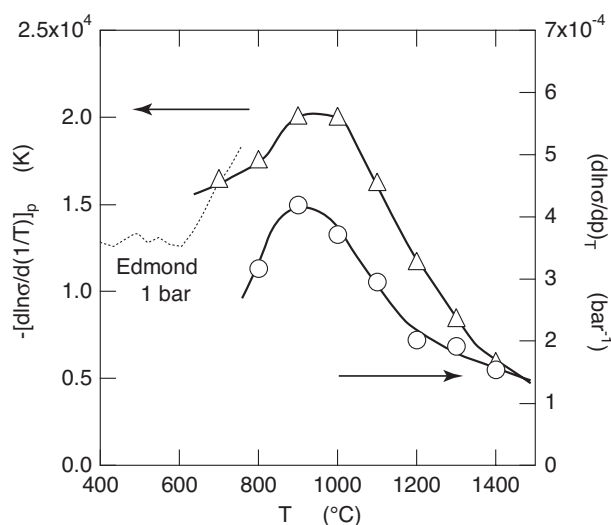
Figure 9. Triangles show the temperature derivatives of σ, $-[d \ln \sigma/d(1/T)]_p$, at a constant pressure of 600 bar. Also given by a dashed curve is $-[d \ln \sigma/d(1/T)]_p$ at normal pressure obtained from [13]. Circles indicate the pressure derivatives of σ, $(d \ln \sigma/dp)_T$, at constant temperatures.

normal pressure measured by Edmond [13]. The σ data under high pressure are slightly larger than Edmond's ones at normal pressure, which cannot be explained by the pressure effect. This difference would originate from an error in the calibration of the sample cell for the σ measurements and/or a formation of small vapour babbles in the sample at normal pressure near the boiling point of As_2Se_3. When the temperature is raised, σ increases significantly. In the semiconductor region below 700 °C, σ increases almost linearly, i.e., the derivative of the curves (the activation energy or the apparent energy gap) seems to be constant. With rising temperature, the slope becomes large at about 900–1000 °C, and at about 1100 °C the σ value reaches the so-called minimum metallic conductivity, some 100 Ω^{-1} cm^{-1}, of Mott's criterion [33]. With the further increase of the temperature, σ increases further but the slope again becomes small.

Triangles in figure 9 show the temperature derivatives of σ, $-[d \ln \sigma/d(1/T)]_p$, at a constant pressure of 600 bar [34], i.e., the slope of σ in figure 8. Also given by a dashed curve is $-[d \ln \sigma/d(1/T)]_p$ at normal pressure obtained from [13]. At low temperatures below 600 °C, a constant value of about 1.3×10^4 K can be obtained for the slope. Beyond this, the value starts to increase rapidly. As mentioned above, the slope shows a maximum around 950 °C. Circles in figure 9 indicate the pressure derivatives of σ, $(d \ln \sigma/dp)_T$, at constant temperatures. As also observed in other liquid chalcogens [25, 35], $(d \ln \sigma/dp)_T$ show a maximum at about 900 °C, near the SC–M transition range. This anomaly suggests a substantial change in the local atomic configuration in liquid As_2Se_3.

Figure 10 shows the logarithmic plots of optical absorption coefficient α of liquid As_2Se_3 as a function of photon energy, $\hbar\omega$, at various temperatures up to 900 °C at 20 bar. The spectra for the glassy and supercooled liquid phases are also presented. Our result for glassy As_2Se_3 at room temperature is in good agreement with the previous data by Edmond [13]. He also measured α of liquid As_2Se_3 in a limited low absorption range from 5 to 2×10^2 cm^{-1}. Our results are again in good agreement with his data in the absorption range around 10^2 cm^{-1}, but less consistent in the lower absorption region.
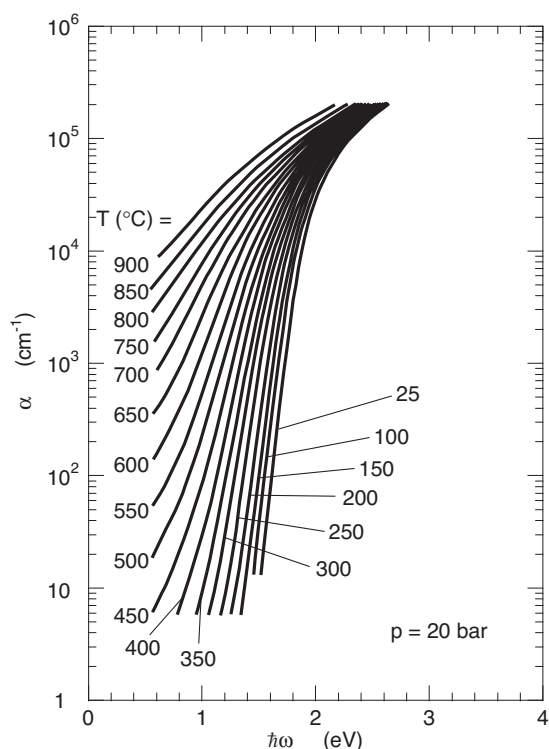
Figure 10. Logarithmic plots of optical absorption coefficient α of liquid As_2Se_3 as a function of photon energy, $\hbar\omega$, at various temperatures up to 900 °C at 20 bar. The spectra for the glassy and supercooled liquid phases are also presented.

The α curves shown in the figure can be separated into three parts as usually seen in amorphous semiconductors: a weak shoulder in the low absorption region, the intermediate part with an exponential variation, and the high absorption part with a power dependence on photon energy. As clearly seen in the figure, the α curve shifts to the low energy side with increasing temperature. It should be noted that all curves up to about 800 °C in the high absorption region seem to be converged on a fixed point at about 3.2 eV and 4×10^5 cm^{-1}, while those at higher temperatures shift almost in parallel.

From a detailed analysis of these spectra in the high-absorption region, we obtained the optical gap, E_g, defined by the conventional relation $(\alpha\hbar\omega)^n \propto \hbar\omega - E_g$, where n is a constant. It is well known that n is 1/2 in glassy As chalcogenides, while amorphous Se has $n = 1$ [33], which is believed to be due to the low dimensionality of amorphous Se. The temperature variation of E_g for As_2Se_3 is shown in figure 11, and the values of E_g and the corresponding n are summarized in table 1. It should be noted that the n value starts to decrease at 500 °C. Triangles in the figure show the energies at which α becomes 3×10^3 cm^{-1}. This is also a conventional way to determine E_g. It is interesting that both values show an almost identical temperature dependence. As seen in the figure, E_g decreases rapidly with increasing temperature, eventually becoming zero at about 950 °C, where the SC–M transition occurs.

The σ value where E_g becomes zero or the bandgap closes is only about 20 Ω^{-1} cm^{-1}, which is much smaller than the minimum metallic conductivity of some 100 Ω^{-1} cm^{-1} proposed by Mott [33] for normal three-dimensional non-crystalline systems. It should be
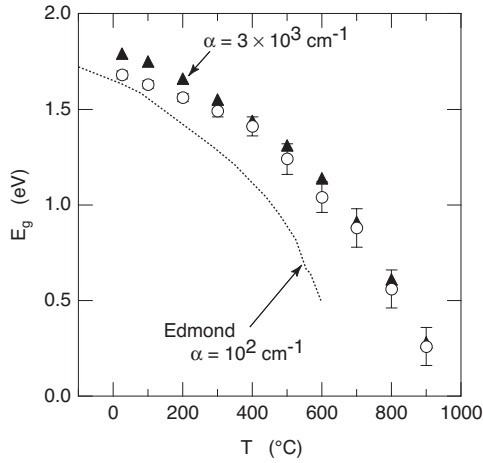
Figure 11. Temperature variation of E_g for As_2Se_3 determined by a conventional relation $(\alpha\hbar\omega)^n \propto \hbar\omega - E_g$. Triangles show the energies at which α becomes 3×10^3 cm^{-1}.
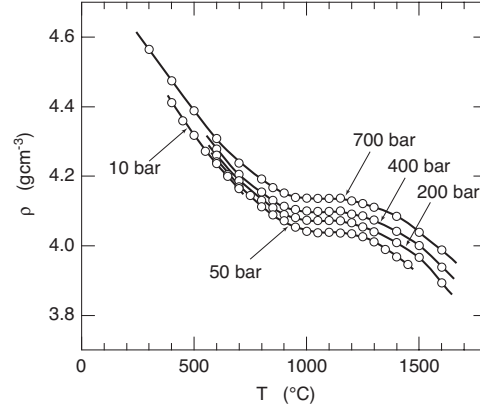
**Figure 12.** Density, ρ, of liquid As_2Se_3 at constant pressures as a function of temperature.

Table 1. The values of E_g and n obtained using the conventional relation $(\alpha\hbar\omega)^n \propto \hbar\omega - E_g$, together with the value of energy where α becomes 3×10^3 cm^{-1}, E_α.

T (°C)	E_g	n	E_α
25	1.68	0.50	1.79
100	1.63	0.50	1.75
200	1.56	0.50	1.66
300	1.49	0.50	1.55
400	1.41	0.50	1.44
500	1.24	0.45	1.31
600	1.04	0.40	1.14
700	0.88	0.40	0.91
800	0.56	0.33	0.61
900	0.26	0.30	0.28

noted that such a small σ value was also seen in expanded liquid Se [36]. Mott and Davis [37] and Mott [38] again predicted that this value of minimum metallic conductivity could not be adapted to low-dimensional systems, and instead a value of some 10 Ω^{-1} cm^{-1} can be reasonable for one-dimensional systems. This intuitive speculation indirectly supports the chain-like structure of high-temperature metallic As_2Se_3.

3.2. Thermodynamic property

Figure 12 shows the density ρ of liquid As_2Se_3 at constant pressures as a function of temperature. In the semiconducting region below 800 °C, ρ decreases almost linearly with increasing temperature. When the SC–M transition region is approached, however, the rate of decrease in ρ becomes small, and is eventually almost zero in the temperature range from 950 to 1250 °C. Thus, it is obvious that a substantial volume contraction occurs in parallel with the normal thermal expansion. The volume contraction accompanied by the SC–M transition can be estimated to be more than 10%. With a further increase of the temperature, ρ starts
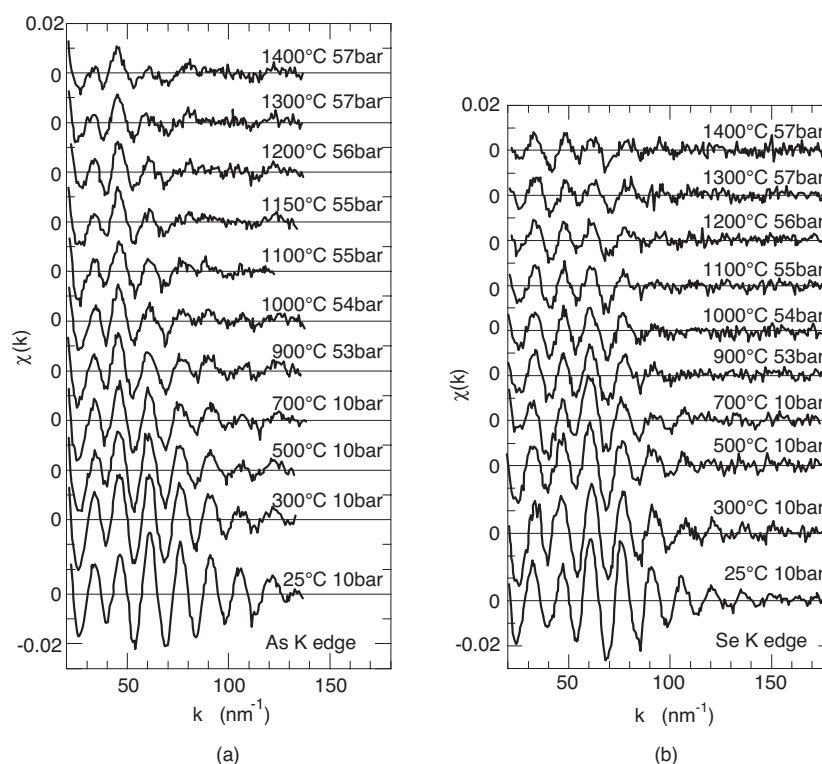
Figure 13. XAFS oscillations, $\chi(k)$, obtained around the (a) As and (b) Se K edges for liquid As$_2$Se$_3$ at various temperatures up to 1400 °C, together with those for glassy As$_2$Se$_3$ at 25 °C and 10 bar.

to decrease again. On applying pressure, the temperature range where ρ is almost constant is slightly shifted to lower temperature, which suggests that the SC–M transition occurs at lower temperature under a higher pressure.

3.3. Structure

Figures 13(a) and (b) show the XAFS functions, $\chi(k)$, obtained around the As and Se K edges, respectively, for liquid As$_2$Se$_3$ at various temperatures up to 1400 °C and the corresponding pressures up to about 60 bar. Also given are those for the glassy state at 25 °C and 10 bar. Distinct XAFS oscillations remain even at the highest temperature of 1400 °C.

Figures 14(a) and (b) show the magnitude of the Fourier transforms of $k\chi(k)$, $|F(r)|$, obtained around the As and Se K edges, respectively. The main sharp peaks for the glassy phase correspond to the As–Se covalent bonds. With increasing temperature in the semiconducting region below 1000 °C, the height of the main peak becomes small while the peak positions are almost unchanged. When the SC–M transition region is approached, however, remarkable structural changes take place: the main peak in $|F(r)|$ from the As K-edge data shown in figure 14(a) suddenly broadens at about 1100 °C. With a further increase of temperature, it becomes much broader. On the other hand, that from the Se K edge shown in figure 14(b) seems to exhibit no substantial change on the SC–M transition.

The structural parameters, such as nearest-neighbour distance r_1, coordination number N_1, and root-mean-square displacement σ_1, for the neighbouring atoms around the central As
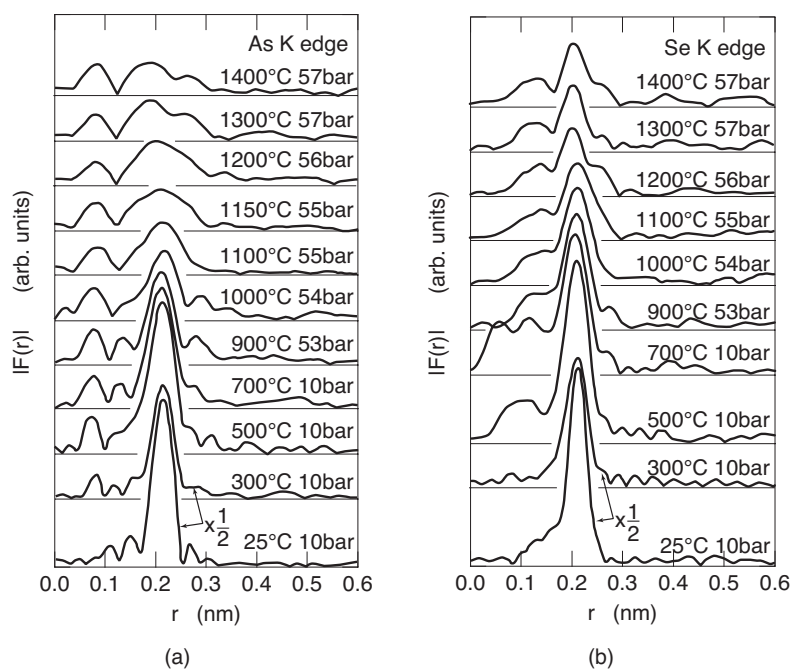
Figure 14. Magnitudes of the Fourier transform of $k\chi(k)$, $|F(r)|$, around the (a) As and (b) Se K edges.

and Se atoms were determined by curve fits using the standard Fourier filtering technique [39]. Curve fits were carried out by assuming that the nearest neighbours around the central atoms in liquid As_2Se_3 are unlike atoms, and they have one Gaussian distribution. This curve fit could successfully be applied to all of the data except the following. At temperatures beyond 1150 °C, the quality of the fits to the spectra taken around the As K edge was inferior, as expected from the broad shape of the main peak in $|F(r)|$ shown in figure 14(a). For these data, we performed curve fits assuming that there are two types of site for nearest neighbours around the central As atom: an Se site and an As one. The Se site is essentially the same as that in the original As–Se covalent bond. An additional As site was considered on the following basis. As seen in figure 14, when the SC–M transition occurs, a broadening of the main peak in $|F(r)|$ was clearly observed only around the central As atom but not around the Se atom. This distinct difference led us to a reasonable assumption that the second site around the central As atom must be an As atom, which gives new As–As bonds.

In figure 15(a), open circles and triangles denote r_1 for the As–Se bonds obtained from the curve fits to the spectra taken around the As and Se edges, respectively, as a function of temperature. The obtained r_1 values of about 0.242 nm for glass and liquid near the melting point are in good agreement with the previous x-ray [5] and neutron [11] scattering data. It appears very clear that the consistency between these data is quite good in the semiconducting as well as metallic region. With increasing temperature, r_1 slightly decreases. When the SC–M transition occurs, the new As site around the As atoms appears as indicated by full circles. It is located around 0.26 nm, and its position remains almost unchanged with a further increase of temperature.

The N_1 values obtained are shown in figure 15(b). The symbols correspond to those in figure 15(a). They are normalized by selecting the scaling factors (the ratio of the experimental
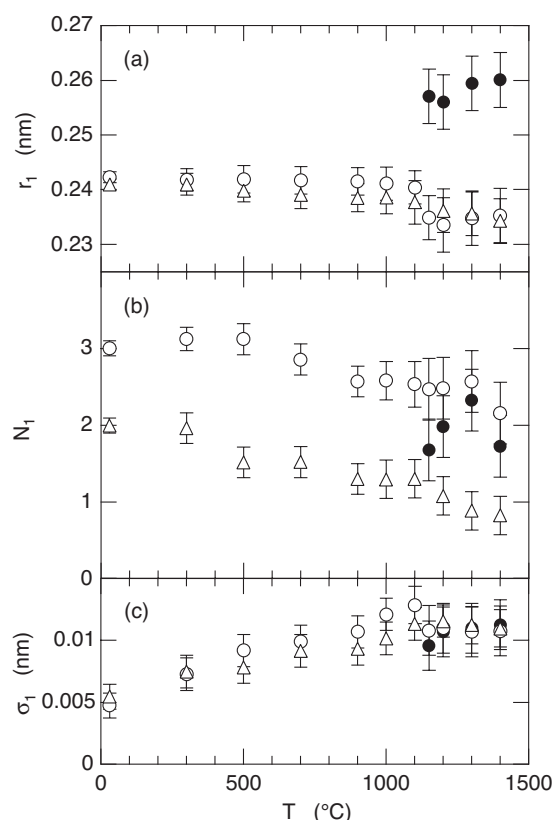
Figure 15. Temperature variation of (a) the nearest-neighbour distance r_1, (b) the coordination number N_1, and (c) the root-mean-square displacement σ_1 for the neighbouring atoms, obtained from the curve fits. Open and full circles respectively indicate the values for Se and As atoms around a central As atom, and open triangles those for As atoms around a central Se atom. See the text for details.

amplitude of $\chi(k)$ to the calculated one) so that for glassy As_2Se_3 the N_1 for the As neighbours around Se and for the Se neighbours around As give the reasonable values of 2 and 3, respectively. With increasing temperature in the semiconducting range, N_1 slightly decreases. When the SC–M transition occurs, N_1 for the As neighbours around As, indicated by closed circles, rapidly increases, eventually becoming comparable to N_1 for the Se neighbours around As (open circles) at 1300 °C.

The σ_1 values obtained are shown in figure 15(c). Again the symbols correspond to those in figure 15(a). The σ_1 values at low temperatures below 600 °C are slightly (10–20%) larger than the previous XAFS data by Crozier *et al* [9], due probably to the limited k range of the present measurements, but the temperature dependences are consistent with each other. The σ_1 values increase with increasing temperature in the semiconducting region, but remain almost unchanged in the metallic range.

Figure 16 shows $S(Q)$ for liquid As_2Se_3 at different temperatures and pressures up to 1600 °C and 80 bar [19]. In the region $Q > 80$ nm^{-1}, the data are rather scattered because of the decrease of the diffracted x-ray intensity with increasing Q. Nevertheless, $S(Q)$ near the melting point is in good agreement with the result of the previous neutron diffraction measurement [11]. With increasing temperature, the oscillations in $S(Q)$ dampen. Especially,
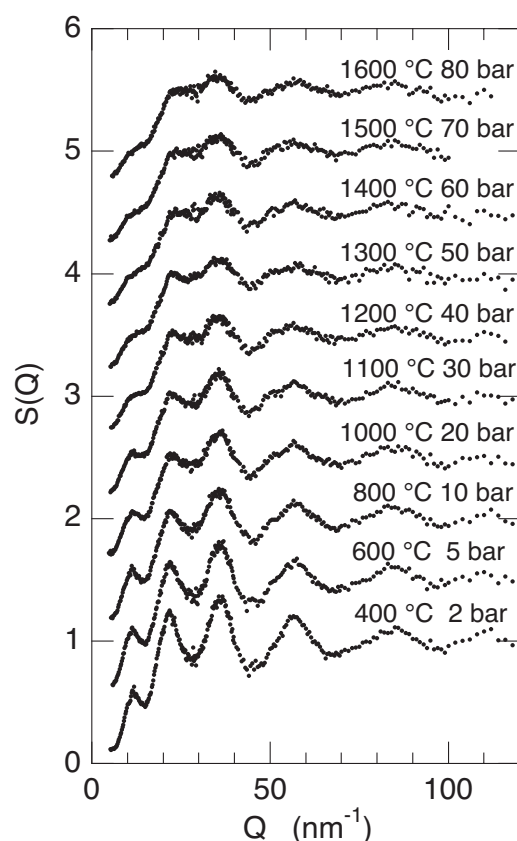
Figure 16. Structure factors, $S(Q)$, of liquid As_2Se_3 at different temperatures and pressures up to 1600 °C and 80 bar. The data are shifted against one another by 0.5.

the first peak around 22 nm^{-1} in $S(Q)$ rapidly becomes broad followed by relatively slow damping of the second peak around 35 nm^{-1}. When the SC–M transition occurs, $S(Q)$ substantially changes: the prepeak around 12 nm^{-1} becomes a shoulder and the first and second maxima start to merge.

The prepeak located at about 12 nm^{-1} is clear evidence for the existence of an IRO with the correlation length of about 0.5 nm, and shows a temperature variation different from other peaks with which the SRO is associated. The relation between the feature of the prepeak and the SC–M transition becomes clear from the present results. The height and the width of the prepeak are almost unchanged in the semiconductor region up to 800 °C, although the other peaks remarkably broaden with increasing temperature. In the SC–M transition region of 1000–1100 °C, the peak height rapidly decreases with temperature. From 1200 °C upward, the prepeak eventually changes to a shoulder. It should be noted that the shoulder or a trace of the intermediate correlation still remains at highest temperature of 1600 °C in the present measurements.

For a detailed study of the prepeak or the IRO, a two-Gaussian fit was attempted for the prepeak (or the shoulder) and the first peak to obtain the width Δ and the area A of the prepeak in $S(Q)$. Figure 17 depicts Δ and A as a function of temperature. With increasing temperature, A decreases slowly and almost linearly even when crossing the SC–M transition range. On the
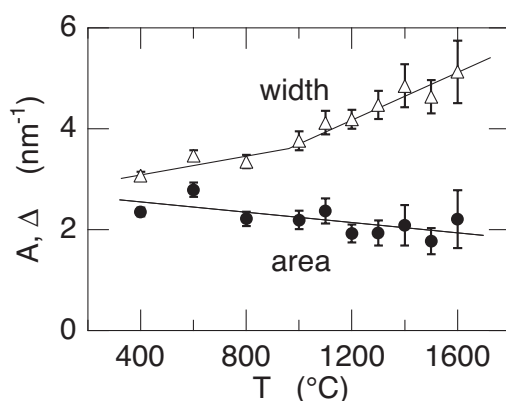
Figure 17. Width Δ and area A of the prepeak in $S(Q)$ for liquid As_2Se_3 are shown by triangles and circles, respectively, as a function of temperature. Lines are a guide for the eyes.

other hand, Δ slightly increases with temperature in the semiconducting region, while rapidly in the metallic range beyond $1000\,°C$. This finding suggests that the change in the shape from the peak to the shoulder on the SC–M transition is not caused by the disappearance of the prepeak but by its rapid broadening. This result is very interesting because the IRO in the semiconducting liquid As_2Se_3 basically survives in the metallic liquid.

Figure 18 shows pair distribution functions, $g(r)$, of liquid As_2Se_3. The $g(r)$ curves were obtained from the Fourier transform of a smooth curve following the experimental points. In the transformation procedure the values of $S(Q)$ in the small Q region between 0 and $5\,nm^{-1}$ were estimated by interpolating the values of $S(0)$ and $S(Q)$ above $5\,nm^{-1}$, $S(0)$ being calculated using the isothermal compressibility obtained from the density data under pressure shown in figure 12. The small peaks in $g(r)$ in the region $r < 0.2\,nm$ are due to the truncation effects in the Fourier transformation. The $g(r)$ curve near the melting temperature is in good agreement with the previous neutron result [11]. With increasing temperature in the semiconducting region, the oscillations in $g(r)$ diminish. Broadening of the first peak at $0.24\,nm$, as well as the second peak around $0.36\,nm$, gradually occurs, but no significant change in the first peak position is observed. When the SC–M transition occurs around $1000\,°C$, the position of the first peak starts to slightly shift towards longer r, and the shape becomes asymmetric.

The SRO in liquid As_2Se_3 was again examined over a wide temperature range including the semiconducting and metallic regions. From the $g(r)$ data given in figure 18, the nearest-neighbour distance, r_1, and the average coordination number, N_1, were obtained as a function of temperature as shown in figure 19 together with the previous data for the glassy As_2Se_3. The values of N_1 were obtained by a usual method of integrating the radial distribution functions, $4\pi r^2 \rho_0 g(r)$, up to the first maximum position and taking twice the integral, where ρ_0 denotes the average number density. The values of r_1 and N_1 at $400\,°C$ are $0.241\,nm$ and about 2.5, respectively, which is in good agreement with the previous neutron values [11]. The N_1 value is nearly equal to the averaged coordination number for crystalline As_2Se_3 of 2.4 [1]. With increasing temperature in the semiconducting region below $1000\,°C$, r_1 remains almost unchanged, and N_1 slightly decreases due to the thermal rupture of the As–Se covalent bonds. When the SC–M transition occurs, on the other hand, r_1 and N_1 start to increase.

From the XAFS measurements, it was found that new As sites at about $0.26\,nm$ appear around the central As atoms in addition to the original Se sites at about $0.24\,nm$, when the SC–M transition occurs. This is consistent with the results of this x-ray diffraction study: the
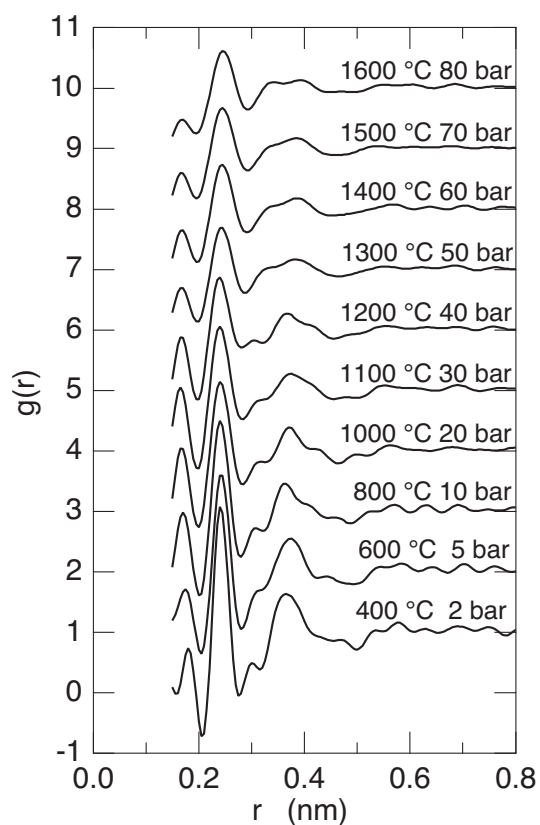
Figure 18. Pair distribution functions, $g(r)$, of liquid As_2Se_3 at different temperatures and pressures up to 1600 °C and 80 bar. The curves are shifted against one another by unity.
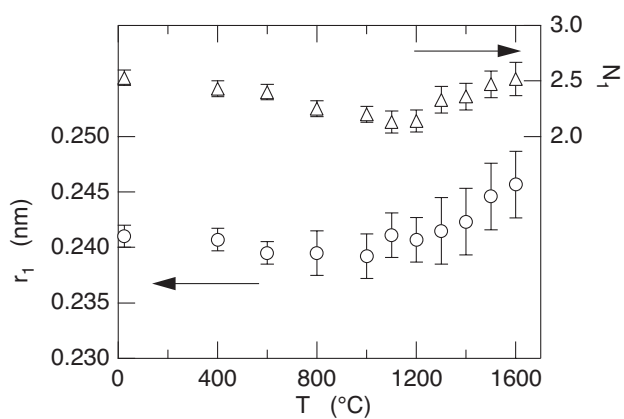
Figure 19. Nearest-neighbour distance r_1 (circles) and the average coordination number N_1 (triangles) for liquid As_2Se_3 as a function of temperature.

formation of the new As–As bonds, which are slightly longer than the original As–Se bonds, causes the asymmetric broadening of the first peak in $g(r)$ and the increase in r_1 and N_1.
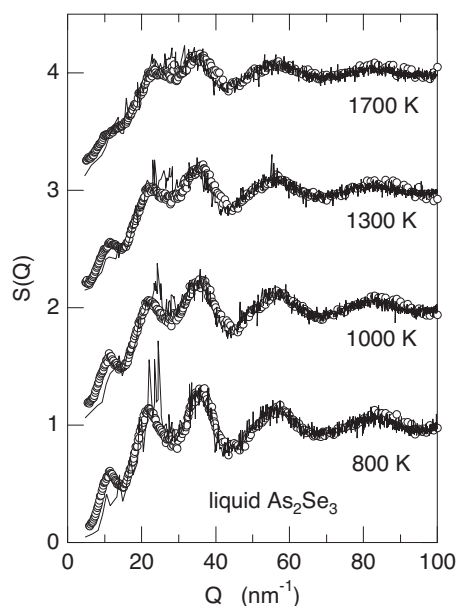
Figure 20. The comparison between the computational $S(Q)$ results (thin solid curves) [21] and the experimental x-ray scattering data (open circles) [19].

4. Discussion

From the present series of the experimental works on liquid As_2Se_3 under high temperature and high pressure, we have found the SC–M transition in this system at about $1000\,°C$ accompanied by the distinct structural changes together with the thermodynamic anomaly (apparent volume contraction) across this electrical transition. The break-down of the IRO (or the chemical short-range order) on the SC–M transition is clearly seen in both the structural results of the x-ray diffraction and XAFS measurements. For the further understanding of this transition, theoretical investigations are very useful. In this section, we will discuss this temperature-driven SC–M transition with help of an *ab initio* MD simulation. We will also point out some limitations of the theoretical calculation for this liquid system.

It is well known that an *ab initio* or first-principles MD simulation has revealed a strong feasibility for investigating structural, electronic, and dynamic properties of many non-crystalline systems since Car and Parrinello [40] proposed this technique about two decades ago. Shimojo *et al* [21, 22] applied this theoretical technique to liquid As_2Se_3 under high temperature and high pressure. Figure 20 shows the comparison of the computational $S(Q)$ results with the experimental x-ray diffraction data. The solid curves show the calculated $S(Q)$, and the open circles the experimental results [19]. The former is taken from figure 1 of [21], and the newly obtained data are drawn for the latter, in which the $S(Q)$ data in the lower-Q region are added to the original figure. The computational results are in good agreement with the experimental data. It should, however, be noted that in the semiconducting region the prepeak at $Q \sim 12\ \text{nm}^{-1}$ obtained experimentally is not well reproduced by the theory. This suggests that the calculated atomic structure describes well the SRO over the wide temperature range, but does not reproduce the IRO of this liquid system. This discrepancy may happen because of the limited spatial size, 1.34–1.38 nm, of this *ab initio* MD simulation [21, 22], which is slightly larger than twice the correlation length at the prepeak position, $r = 2\pi/Q_{\text{prepeak}} \sim 0.52\ \text{nm}$.
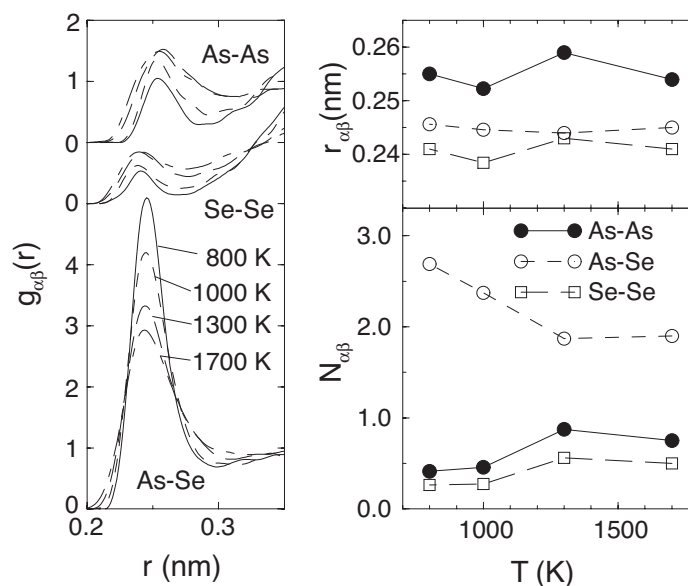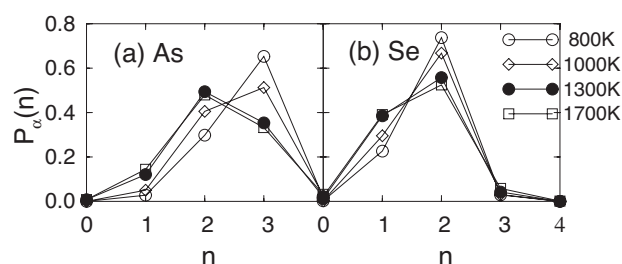
Figure 21. Partial pair distribution functions, $g_{\alpha\beta}(r)$, partial bond lengths, $r_{\alpha\beta}$, and partial coordination numbers, $N_{\alpha\beta}$, obtained by the *ab initio* MD simulation [22].

Here, we will discuss the SRO of the theoretical results by comparing to the x-ray scattering and XAFS results, and then return to the prepeak or the IRO.

Figure 21 shows partial pair distribution functions, $g_{\alpha\beta}(r)$, partial bond lengths, $r_{\alpha\beta}$, and partial coordination numbers, $N_{\alpha\beta}$, obtained by the calculation. The figure is taken from figure 4 of [22]. The computational results revealed that in the semiconductor regime the system strongly prefers bonds between the unlike atoms, i.e., As–Se bonds as assumed in the present x-ray scattering and XAFS experiments. However, there are small portions of the wrong bonds, i.e., As–As or Se–Se bonds, which the experiments could not detect. With increasing temperature, these wrong bond portions rapidly increase when crossing the SC–M transition. The existence of a large number of As–As wrong bonds was observed by our XAFS experiment, whereas that of Se–Se bonds could not be detected. This is due to the Se–Se bond length being closely similar to the As–Se one as pointed out by Shimojo *et al* [21, 22], and the very similar backscattering amplitude and phase shift functions between the As and Se elements. Namely, it is hard for the XAFS technique to discriminate the As and Se neighbours if the bond lengths are very similar to each other. The existence of the longer As–As bonds was clearly observed by our XAFS and x-ray scattering experiments as seen in figures 15 and 19, respectively.

As regards the temperature dependence of the coordination number, the theoretical results indicate the almost unchanged averaged coordination number of $\sim$2.5. This contradicts the present x-ray diffraction result in the high-temperature metallic region, where it shows the distinct increase of the averaged coordination number. However it should be noted that with increasing temperature the shape of the first peak in each $g_{\alpha\beta}(r)$ becomes highly asymmetric especially when crossing the SC–M transition, while Shimojo *et al* [21, 22] calculated the coordination number as twice $4\pi r^2 g_{\alpha\beta}(r)$ up to the peak position of $g_{\alpha\beta}(r)$, i.e., the distribution is assumed to be symmetric. The disagreement between the theory and the experiment comes from this method of obtaining the coordination number.

Figure 22. Coordination distribution functions, $P_\alpha(n)$, around the (a) As and (b) Se atoms.

The most interesting result obtained from the MD simulation on the SRO is the coordination number distribution around the As atoms. Figure 22 shows the coordination distribution functions, $P_\alpha(n)$, around the (a) As and (b) Se atoms. The figure is taken from figure 5 of [22]. When crossing the SC–M transition, the number of threefold coordinated As is highly suppressed, and the twofold coordinated As atoms remarkably increase. On the other hand, the twofold coordinated Se atoms still dominate in the $P_{Se}(n)$, although the onefold coordinated Se atoms or the dangling bonds slightly increase with increasing temperature. As a result, a major part of this liquid mixture at higher temperatures consists of a twofold coordinated chain-like structure formed by both the As and Se atoms.

Based on these simulated structural data, Shimojo *et al* [21, 22] calculated the temperature dependence of the total and partial electronic density of states (DOS) for each coordination number. The results are given in figure 9 of [22]. From this figure, we see that at low temperatures each DOS at the Fermi level, E_F, has a steep dip, which seems to be independent of the local coordination. With increasing temperature, the dip in each partial DOS is gradually filled up. It should be noted that the contributions to the DOS with lower-coordinated atoms precede those with higher-coordinated atoms for increasing value at E_F. This fact clearly demonstrates that the electronic states around lower-coordinated atoms are very important for the metallization of this liquid.

Shimojo *et al* [21, 22] also demonstrate the partial distribution of the electronic wavefunctions with eigenenergies near the E_F as well as the chain-like atomic configurations in figure 10 of [22]. It is clearly seen in this figure that the electronic wavefunctions have a large amplitude around the twofold coordinated As and Se atoms. This spatial distribution is similar to that of the p-like nonbonding orbitals in fluid Se calculated by Shimojo *et al* [41]. In the metallic region for the fluid Se, the dihedral angle has a flatter distribution, but a plateau can still be recognized. Thus, Shimojo *et al* [41] concluded that the helical chain structure persists in fluid Se even in the metallic phase. This may come from the repulsive force between the non-bonding p orbitals of neighbouring Se atoms. In the case of liquid As_2Se_3, a zigzag structure can be recognized around the As atoms as shown in figure 10 of [22], where the lack of the p electron at the As atoms in the chain structure partially results in the attractive force between nonbonding states along the chain (π bonds). The existence of small chain molecules with a planar zigzag conformation was speculated in our paper on metallic fluid Se [42], and was illustrated in figure 8 of [43] and figure 2 of [44]. A detailed analysis of the dihedral angle distribution around the twofold coordinated As atoms is necessary to confirm the above observation.

Before discussing the temperature dependence of the IRO or the prepeak in $S(Q)$, it is useful to introduce a recent work that explored its origin in glassy As_2Se_3 by means of anomalous x-ray scattering (AXS) [45]. The occurrence of the prepeak around 12 nm^{-1} in
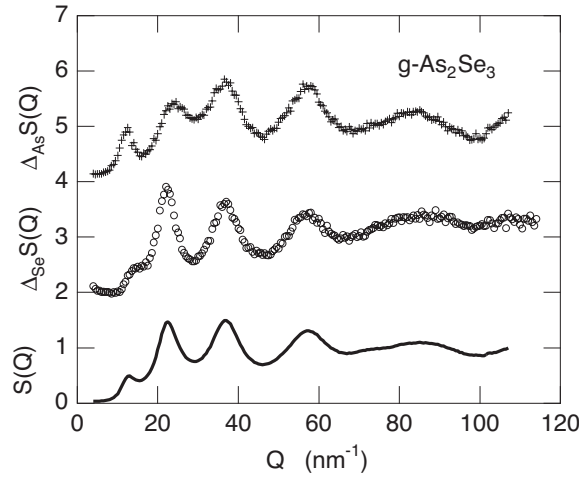
Figure 23. Differential structure factors, $\Delta_i S(Q)$, of glassy As_2Se_3 close to the As (crosses) and Se (circles) K edges together with $S(Q)$ measured at 200 eV below the As K edge (solid curve).

Table 2. Weighting factors, W_{ij}, given for $\Delta_i S(Q)$ around the As and Se K edges, together with those for $S(Q)$ at $Q = 22.5$ nm^{-1} (the first maximum position in $S(Q)$).

	$\Delta_{As} S(Q)$	$\Delta_{Se} S(Q)$	$S(Q)$
W_{AsAs}	0.328	−0.038	0.143
W_{AsSe}	0.604	0.404	0.470
W_{SeSe}	0.068	0.634	0.387

$S(Q)$ in glassy As_2Se_3 obtained by diffraction methods presents clear evidence for the existence of an IRO. In order to clarify the role of each constituent for the IRO in glassy As_2Se_3, AXS experiments were recently carried out. In this work, differential structure factors, $\Delta_i S(Q)$, were derived from a detailed analysis of the x-ray scattering data close to the As and Se K edges. The experiments were performed at two energies below each K edge (20 and 200 eV below the As K edge of 11 867 eV and the Se K edge of 12 658 eV) at beamline BM02 of the European Synchrotron Radiation Facility (ESRF) in Grenoble, France. In a binary system, $\Delta_i S(Q)$ can be written as a linear combination of three partial structure factors, $S_{ij}(Q)$, each weighted by a factor,

$$W_{ij}(Q, E) = c_i c_j \Delta_A (f_i(Q, E) f_j^*(Q, E)) / \Delta_A (\langle f(Q, E) \rangle^2).$$

Here, c_i is the concentration, $\Delta_A( )$ is the difference of the function in the parentheses close to the A edge, $\langle \rangle$ is the chemical average, and $f_i(Q, E) = f_{0i}(Q) + f_i'(E) + i f_i''(E)$ is the complex atomic form factor of the ith element, where f_{0i} is the usual energy-independent term and f_i' and f_i'' are the real and imaginary parts of the anomalous contributions, respectively. In table 2, the W_{ij} values are given for $\Delta_i S(Q)$s close to the As and Se K edges together with those for $S(Q)$ at $Q = 22.5$ nm^{-1} (the first maximum position in $S(Q)$). They slightly vary with changing Q.

Figure 23 shows $\Delta_i S(Q)$s of glassy As_2Se_3 close to the As (crosses) and Se (circles) K edges. For comparison, $S(Q)$ measured at 200 eV below the As K edge is also shown by a solid curve in the figure. $\Delta_{As} S(Q)$ has a distinct and sharp prepeak around $Q = 12$ nm^{-1}, the position of which almost coincides with that in $S(Q)$ although the latter is much broader. Any

structure at this Q value can hardly be seen in $\Delta_{Se}S(Q)$, while $\Delta_{Se}S(Q)$ shows a shoulder at a higher Q value of 14.5 nm^{-1}, where $\Delta_{As}S(Q)$ has no indication. It should be noted that as shown in table 2 the contribution of $S_{SeSe}(Q)$ is very small in $\Delta_{As}S(Q)$ and that of $S_{AsAs}(Q)$ is negligible in $\Delta_{Se}S(Q)$. Therefore, it appears plausible that the main part of the prepeak at $Q \sim 12$ nm^{-1} originates from the As–As correlation, and its higher-Q side around 14.5 nm^{-1} from the Se–Se correlation.

It was believed for a long time that the prepeak at $Q = Q_p \sim 12$ nm^{-1} indicated the existence of an IRO with a correlation length $r = 2\pi/Q_p \sim 0.52$ nm in real space. Several models were proposed to explain the origin of this correlation, such as a layer structure similar to the crystal, clusters, or voids. However, no special indication of the correlation was found at the length of 0.52 nm in $g(r)$ or $\Delta_i g(r)$s [45]. Therefore, the origin of the prepeak should be considered in a different way, similar to the speculation for glassy GeSe$_2$ [46]. The interatomic distance of the As–(Se)–As is well defined to be $\sim$0.367 nm, and the second shell around an As atom contains three As neighbours. If the atomic arrangement of this As sub-lattice has an amorphous As-like structure [47], $S_{AsAs}(Q)$ should have a peak at a Q position corresponding to the first peak position in $S(Q)$ of amorphous As, 21.9 nm^{-1}. The scaling factor can be given by the ratio of the As–As interatomic distances, 0.245/0.367. The resultant Q_p position is 14.6 nm^{-1}, which is larger than the present value, 12 nm^{-1}. Although a modification of the As sub-lattice from the amorphous As configuration is needed for the quantitative analysis, this idea itself seems to be promising for the understanding of the origin of the prepeak.

As we can see in figure 20, the reproducibility of the computational results is bad in the low-Q region around the prepeak position of 12 nm^{-1}, where the prepeak in this region results from the As–As correlation in the glassy state. On the other hand, it is relatively good at the dip between the pre- and first peaks all over the wide temperature range, where the Se–Se correlation dominates in the glassy state. This result may suggest that the size for the MD calculation is enough for the correlation length of the Se–Se partial IRO, but insufficient to perfectly reproduce the As–As partial IRO.

This *ab initio* MD simulation has another point that is insufficient to understand the temperature driven SC–M transition in liquid As$_2$Se$_3$ although the experimental result distinctly visualizes it: why the system shows the apparent volume contraction on the transition. In the simulation procedure, the density data were used as input parameters to describe the atomic and electronic structures of the liquids. Several results obtained by this simulation seem to have given us no hints for this thermodynamic anomaly. The same comment can also be claimed to the previous *ab initio* MD calculation on fluid Se [41], for which some experiments [29, 48] realized a thermodynamic anomaly on the SC–M transition, i.e., bends of isochore curves. Except for these insufficiencies, however, this MD simulation shows great feasibilities as reviewed in this section, and has no inconsistencies with our several experimental results.

More recently, investigations of a similar glass-forming liquid GeSe$_2$ have intensively been performed by a neutron scattering experiment [49] and an *ab initio* MD calculation [50, 51]. Their studies were concentrated to the structural changes on the SC–M transition, which is also observed at an elevated temperature of 1000–1100 °C. In particular, the breakdown of the IRO in liquid GeSe$_2$ was carefully discussed experimentally and theoretically. However, further experimental and theoretical studies on electronic structures and thermodynamic properties are necessary to explore universalities and differences between two chalcogenide liquids, As$_2$Se$_3$ and GeSe$_2$. The former mean the universalities between the liquids whose glassy and low-temperature forms have well chemically ordered SRO, and the latter the differences between the liquids whose concentrations are located at the floppy–rigid stiffness transition region (As$_2$Se$_3$) and in the rigid region (GeSe$_2$) of the Philip–Thorpe criterion [2, 3].

5. Summary

Intensive experimental investigations have been performed on a typical liquid semiconductor As_2Se_3 over a wide temperature range under pressure, such as electrical conductivity, optical absorption coefficient, density, XAFS, and x-ray diffraction measurements. With increasing temperature, liquid As_2Se_3 undergoes an SC–M transition at about $1000\,^\circ$C, which is clearly observed by the electrical conductivity and optical absorption measurements. The volume of the system apparently contracts near the transition temperature. The structural changes are observed especially in the IRO or the prepeak in $S(Q)$ characteristic to this glass-forming liquid. The XAFS and x-ray scattering results strongly suggest the new formation of the As–As bonds in addition to the original As–Se bonds in the high-temperature metallic region. The experimental results are carefully discussed by comparing to an *ab initio* MD simulation. Several new insights can be realized from this computational work. A small portion of homopolar bonds already exist in the semiconducting region, and twofold coordinated As atoms existing in a chain structure with twofold coordinated Se atoms plays a very important role for the metallization of this liquid. Some limitations of the MD simulation are also pointed out.

Acknowledgments

References

[1] Vaipolin A A and Porai-Koshits E A 1960 *Sov. Phys.—Solid State* **2** 1500
    Vaipolin A A and Porai-Koshits E A 1963 *Sov. Phys.—Solid State* **5** 178
[2] Phillips J C 1979 *J. Non-Cryst. Solids* **34** 153
    Phillips J C 1981 *J. Non-Cryst. Solids* **43** 37
[3] Thorpe M F 1983 *J. Non-Cryst. Solids* **57** 355
[4] See for example, Mott N F and Davis E A 1979 *Electronic Properties in Non-Crystalline Materials* (Oxford: Clarendon) pp 442–516
[5] Renninger A L and Averbach B L 1973 *Phys. Rev.* B **8** 1507
[6] Chang J and Dove D B 1974 *J. Non-Cryst. Solids* **16** 72
[7] Sagara Y, Uemura O, Okuyama S and Satow T 1975 *Phys. Status Solidi* a **31** K33
[8] Vaipolin A A 1965 *Kristallografia* **10** 596
[9] Crozier E D, Lytle F W, Sayers D E and Stern E A 1977 *Can. J. Chem.* **55** 1968
[10] Schottmiller J, Tabak M, Lucovsky G and Ward A 1970 *J. Non-Cryst. Solids* **4** 80
[11] Uemura O, Sagara Y, Muno D and Sotow T 1978 *J. Non-Cryst. Solids* **30** 155
[12] Taylor P C, Bishop S G and Miychell D L 1971 *Phys. Rev. Lett.* **27** 414
[13] Edmond J T 1966 *Br. J. Appl. Phys.* **17** 979
[14] Nemilov S V 1964 *Sov. Phys.—Solid State* **6** 1075
[15] Kadoun A, Chaussemy G, Fornazero J and Mackowski J M 1983 *J. Non-Cryst. Solids* **57** 101
[16] Hoshino H, Miyanaga T, Ikemoto H, Hosokawa S and Endo H 1996 *J. Non-Cryst. Solids* **205–207** 43
[17] Hosokawa S, Sakaguchi Y, Hiasa H and Tamura K 1991 *J. Phys.: Condens. Matter* **3** 6673
[18] Hosokawa S, Sakaguchi Y and Tamura K 1992 *J. Non-Cryst. Solids* **150** 35
[19] Hosokawa S and Pilgrim W-C 2001 *Phys. Status Solidi* b **223** 145
[20] Tamura K, Hosokawa S, Inui M, Yao M, Endo H and Hoshino H 1992 *J. Non-Cryst. Solids* **150** 351
[21] Shimojo F, Munejiri S, Hoshino K and Zempo Y 1999 *J. Phys.: Condens. Matter* **11** L153
[22] Shimojo F, Munejiri S, Hoshino K and Zempo Y 2000 *J. Phys.: Condens. Matter* **12** 6161

[23] Hensel F and Franck E U 1966 *Ber. Bunsenges. Phys. Chem.* **70** 1154
[24] Tamura K, Inui M and Hosokawa S 1999 *Rev. Sci. Instrum.* **70** 144
[25] Hoshino H, Schmutzler R W and Hensel F 1976 *Ber. Bunsenges. Phys. Chem.* **80** 27
[26] Hosokawa S, Matsuoka T and Tamura K 1994 *J. Phys.: Condens. Matter* **6** 5273
[27] Sakaguchi Y and Tamura K 2000 *Rev. Sci. Instrum.* **71** 494
[28] For example, Thurn H and Ruska J 1976 *J. Non-Cryst. Solids* **22** 331
[29] Hosokawa S, Kuboi T and Tamura K 1997 *Ber. Bunsenges. Phys. Chem.* **101** 120
[30] Tamura K, Inui M, Yao M, Endo H, Hosokawa S, Hoshino H, Katayama Y and Maruyama K 1991 *J. Phys.: Condens. Matter* **3** 7495
[31] For example, Waseda Y 1980 *The Structure of Non-Crystalline Materials* (New York: McGraw-Hill)
[32] Hosokawa S and Pilgrim W-C 2001 *Rev. Sci. Instrum.* **72** 1721
[33] Mott N F and Davis E A 1979 *Electronic Properties in Non-Crystalline Materials* (Oxford: Clarendon)
[34] Hoshino H, Hosokawa S and Endo H 1981 unpublished
[35] Yao M, Misonou M, Tamura K, Ishida K, Tsuji K and Endo H 1980 *J. Phys. Soc. Japan* **48** 109
[36] Hosokawa S and Tamura K 1990 *J. Non-Cryst. Solids* **117/118** 489
[37] Mott N F and Davis E A 1979 *Electronic Properties in Non-Crystalline Materials* (Oxford: Clarendon) p 187
[38] Mott N F 1990 *Metal–Insulator Transitions* 2nd edn (London: Taylor and Francis) p 241
[39] Teo B K 1986 *EXAFS: Basic Principles and Data Analysis* (Berlin: Springer)
[40] Car R and Parrinello M 1985 *Phys. Rev. Lett.* **55** 2471
[41] Shimojo F, Hoshino K, Watabe M and Zempo Y 1998 *J. Phys.: Condens. Matter* **10** 1199
[42] Tamura K and Hosokawa S 1992 *Ber. Bunsenges. Phys. Chem.* **96** 681
[43] Tamura K 1996 *J. Non-Cryst. Solids* **205–207** 239
[44] Tamura K and Inui M 2001 *J. Phys.: Condens. Matter* **13** R337
[45] Hosokawa S, Wang Y, Bérar J-F, Pilgrim W-C, Mamedov S and Boolchand P 2004 unpublished
[46] Hosokawa S, Wang Y, Bérar J-F, Greif J, Pilgrim W-C and Murase K 2002 *Z. Phys. Chem.* **216** 1219
[47] Bellissent R and Tourand G 1976 *J. Physique* **37** 1423
[48] Fischer R, Schmutzler R W and Hensel F 1980 *J. Non-Cryst. Solids* **35/36** 1295
[49] Petri I, Salmon P S and Howells W S 1999 *J. Phys.: Condens. Matter* **11** 10219
[50] Massobrio C, van Roon F H M, Pasquarello A and De Leeuw S W 2000 *J. Phys.: Condens. Matter* **12** L697
[51] Massobrio C, Pasquarello A and Car R 2001 *Phys. Rev.* B **64** 144205